Renewable Energy 166 (2020) 35–44

Contents lists available at ScienceDirect

Renewable Energy

journal homepage: www.elsevier.com/locate/renene

K_2CO_3 in closed heat storage systems

Jelle Houben [a], Leyla Sögütoglu [a], Pim Donkers [b], Henk Huinink [a, *], Olaf Adan [a, b]

[a] Eindhoven University of Technology, Den Dolech 2, 5600, MB Eindhoven, the Netherlands
[b] TNO Materials Solutions, High Tech Campus 25, 5656, AE Eindhoven, the Netherlands

ARTICLE INFO

Article history:
Received 6 October 2019
Received in revised form
12 November 2020
Accepted 20 November 2020
Available online 25 November 2020

Keywords:
Potassium carbonate
Thermochemical material
Metastable zone
Closed vacuum system
Non-condensable gasses

ABSTRACT

Potassium carbonate, K_2CO_3, has been identified as one of the most promising thermochemical storage materials for the built environment. Where a lot of knowledge has been gained on hydration/dehydration behavior at atmospheric (open system) conditions, little is known of this process under pure water vapor conditions (closed vacuum system). In this paper, for the first time, the equilibrium behavior and reaction kinetics of a K_2CO_3 composite are investigated under pure water vapor conditions, as present in closed vacuum systems. In this work the metastable behavior of a K_2CO_3 composite is investigated under vacuum conditions and compared to its metastable behavior under atmospheric conditions. It is found that the metastable zone is also present in vacuum conditions, however induction times in the metastable zone are much shorter which indicates a faster nucleation rate in vacuum conditions.

Moreover the effect of inert gasses in a closed system is studied and it is shown that it is critical to remove all sources of non-condensable gasses. Finally in cyclic measurements it is shown that K_2CO_3 is stable in multi cyclic experiments, concluding that it is a suitable material for a heat battery based on the concept of a closed reactor.

1. Introduction

The EU is committed to reduce greenhouse gas emissions to 80–95% below 1990 levels by 2050. To achieve this, a transition from fossil to renewable energy has to be made [1]. The development of efficient energy systems is one of the main challenges to make the transition from a fossil based energy society to a renewable based energy society. To increase energy efficiency, the production of energy should be as close as possible to the end user, thereby mitigating conversion and transport losses. These decentralized energy options include combined heat and power, district heating and cooling, geothermal, biomass and solar energy [2]. For these decentralized systems, energy storage is a key component to match demand and supply in time and power. Storage is particularly crucial for thermal energy systems based on solar energy, which often deliver their highest peak during periods of low demand; solar irradiation is high in summer and heat demand is high in winter.

Focusing on the total energy consumption in Northern European countries, 41% can be contributed to the built environment. Of which the largest part can be contributed to thermal energy for residential purposes, resulting in residential thermal energy consuming 25% of the total energy use [3]. Therefore thermal storage in this specific sector may contribute significantly in the reduction of total energy use.

The built environment application also determines the temperature window at which the thermal storage must be charged and discharged. By focusing on residential thermal energy the charge temperature must be lower than 120 °C to be collected by solar panels, and the discharge temperature must be above 50 °C to be used for tap water [4].

A promising heat storage concept is based on thermochemical heat storage, wherein sorption energy is used to store heat via a reversible chemical reaction. Sorption is defined as the fixation or capture of a gas (sorbate) by a solid or liquid (sorbent) [5]. These sorption materials are called thermochemical materials (TCM's). Salt hydrates are a promising subclass of TCM's as they have a high energy density, charge and discharge temperatures suitable for the built environment and a safe sorbate (water vapor) [6].

From an extensive review of 563 hydrate reactions, potassium carbonate (K_2CO_3) has been selected as one of the most promising material for domestic heat storage based on the temperature operating window, stability, price and safety [4]. From the Hazardous Materials Identification System (HMIS), K_2CO_3 scores on all

* Corresponding author.
E-mail address: h.p.huinink@tue.nl (H. Huinink).

https://doi.org/10.1016/j.renene.2020.11.119

Nomenclature

Physics Constants

R	Gas constant 8.314, J/K/mol

Acronyms

MSZ	Metastable Zone
ACS	American Chemical Society
ESD	Energy Storage Density
HMIS	Hazardous Material Identification System
MSDS	Material Safety Data Sheet
NCG	Non Condensable Gasses
SEM	Scanning Electron Microscopy
TCM	Thermochemical Material
TGA	Thermogravimetric Analysis
XRD	X-Ray Diffraction

Other Symbols

ρ_{comp}	composite density, kg/m^3
ρ_{crys}	crystal density, kg/m^3
c_a	concentration in aqueous phase, mol/m^3
H_{cp}	Atmospheric Henry's law constant, mol/m^3/Pa
p	partial pressure, mbar
p_{eq}	equilibrium pressure, mbar
T_{deh}	dehydration temperature, °C
T_{hy}	hydration temperature, °C

points a 1 on a scale from 0 to 4. Indicating minor risks for health, flammability and physical hazard [7]. The Material Safety Data Sheet (MSDS) states that during storage and handling precautions have to be taken, but during commercial use the material is not accessible for the owner of the thermochemical storage owner.

The gas-solid equilibrium reaction for K_2CO_3 is given by:

$$K_2CO_3 + 1.5H_2O(g) \Leftrightarrow K_2CO_3 \cdot 1.5H_2O(s), \quad (1)$$

The reaction from left to right (hydration) is exothermic: energy is released when water is absorbed. And the reaction from right to left (dehydration) is endothermic; heat must be added to desorb the water. For salt hydrates the output temperature is dependent on the supplied water vapor pressure, which is prescribed by the phase diagram. For K_2CO_3 the phase diagram is shown in Fig. 1a, where the 0–1.5 equilibrium line, indicated by lower solid line (red), is taken from Glasser [8]. The dotted line indicates the deliquescence line of K_2CO_3 where the salt goes into solution [9]. And the upper solid line (blue) indicates the liquid-gas equilibrium line of water.

In the Netherlands and other North European countries, the available low source temperature is around 10 °C. This is based on a ground source temperature of 12 °C in a borehole at a depth of 7 m, this can generate a constant temperature of 10 °C at the evaporator of a reactor [11]. In Fig. 1a, a hydration cycle is shown where the lower temperature of 10 °C generates a water vapor pressure of 12 mbar, indicated by the horizontal dashed-dotted line. The maximum hydration temperature of K_2CO_3, can now be determined at the intersect of the horizontal 12 mbar line and the equilibrium phase line of K_2CO_3. Resulting in temperature lift of 50 °C from a low temperature of 10 °C–60 °C.

However in a recent kinetic study by Sögütoglu it is shown that K_2CO_3 and other salt hydrates have a metastable zone [10]. In a metastable zone a nucleation energy barrier limits the hydration and dehydration rates. Metastability indicates that the system is stable to small fluctuations in the thermodynamic variables but that the system will transform in time to the state of a global minimum [12]. To reach this global minimum the system has to overcome an energy barrier. The metastable zone line is the boundary where the nucleation barrier vanishes, as found by Ref. [10] and is shown in Fig. 1b. The practical implication of the metastable zone (MSZ) is that the maximum temperature of discharge is not determined by the equilibrium line, but by the MSZ line for hydration.

For the operation of TCM heat storage two general concepts exist: the open and closed reactor system. A schematic picture is shown in Fig. 2 [4]. An open reactor system operates under atmospheric conditions whereby the heat and mass transport is realized by a forced airflow [13]. The disadvantage of this concept is that the temperature lift is limited and that the operation requires power to drive the forced airflow [14]. The main advantages are the low system complexity [15] and good heat transfer since the transfer fluid is in direct contact with the TCM [16].

A closed system operates under pure water vapor conditions, indicating that the system is vacuumed and the only gas present is water vapor [17]. A closed system consists of a TCM compartment and a liquid water storage vessel. During hydration water vapor is generated by an evaporator and during dehydration water vapor is condensed at the condenser. Usually the evaporator-condenser is a single component. In a closed system mass transport is driven by a pressure difference between water and TCM. The advantages of a closed system are a higher temperature lift and a small amount of energy required for vapor transport [18].

A major disadvantage of a closed system is a rapid decrease in performance when non-condensable gasses (NCG) are introduced. Since NCG will inhibit mass diffusion of water vapor in a closed reactor system [19–21]. This is also shown by Ref. [22] where it was concluded that small partial air pressures in the system deteriorate the charging and discharging process.

NCG can originate from several sources; impurities in the TCM, decomposition of the TCM, gasses dissolved in the water storage vessel and gasses leaking from the ambient into the system [23]. Several widely studied TCM's have issues with thermal stability and decomposition, i.e. $MgCl_2$ and Na_2S. $MgCl_2$ irreversible decomposes and HCl (g) is released [24,25]. Na_2S emits H_2S (g) [26–28]. Although decomposition is not an issue for pure K_2CO_3, impurities of potassium bi-carbonate ($KHCO_3$) can decompose and release CO_2 [28]. $KHCO_3$ impurities can originate from the base material, be introduced during storage and handling or be introduced during an ex-situ re-hydration step of the composite due to CO_2 uptake.

The cyclic stability of K_2CO_3 during hydration/dehydration has been studied under atmospheric condition by Ref. [28], whereby it is shown that K_2CO_3 performs stable over many cycles. However under atmospheric conditions impurities will not affect the operation of the system since mass transport is driven by forced airflow and CO_2 will be removed. This is not the case in a closed system where CO_2 can block the vapor transport [21]. It has been shown by Ref. [29] that CO_2 can be cyclic absorbed, however it is also shown by Ref. [28] that compared to the hydration reaction of K_2CO_3 the carbonation reaction is slow. Therefore CO_2 released in a closed system will compromise the performance of a closed system.

Besides the role of CO_2 in a closed system, also the phase behavior and kinetics of K_2CO_3 is poorly understood. Much knowledge on the hydration/dehydration behavior has been gained under atmospheric conditions [10,28]. Little is known of this process under pure water vapor conditions as present in a closed system (vacuum system).

This paper aims to elucidate the behavior of K_2CO_3 in a closed (vacuum) system. Therefore the equilibrium behavior and reaction

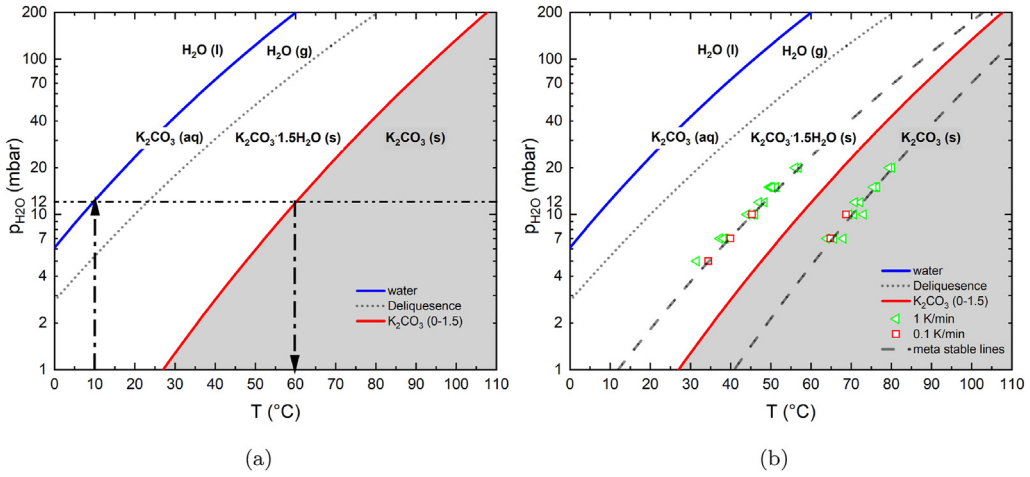

Fig. 1. a) The phase diagram of K_2CO_3. The red solid line is the K_2CO_3 0–1.5 equilibrium line, the dotted line is the deliquescence line of K_2CO_3 and the blue solid line is the liquid-gas equilibrium line of water b): The same phase diagram including the experimentally determined metastable zone by Sögütoglu et al. [10]. The metastable zone is indicated by the dashed lines: the upper dashed line for hydration and the lower for dehydration. The triangles and squares are the experimentally determined onset points at a rate of 1 K/min and 0.1 K/min, respectively. (For interpretation of the references to color in this figure legend, the reader is referred to the Web version of this article.)

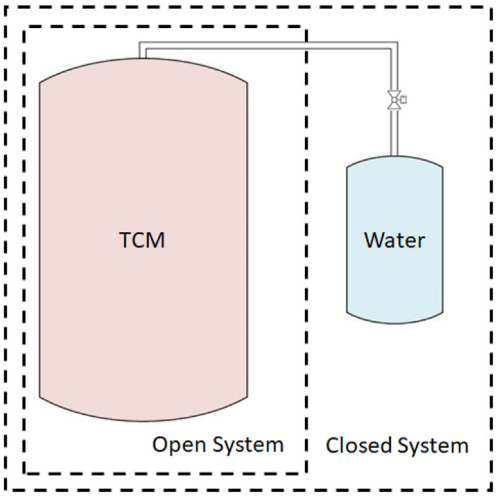

Fig. 2. Schematic representation of a closed and open reactor system. The closed system operates under pure water vapor conditions. In a closed system liquid water is stored inside the system and water vapor is generated internally with an evaporator. In an open system the TCM is operated at ambient pressure in the presence of inert gas (air), the water vapor is supplied to the TCM from an external source. Figure adapted from Refs. [13].

kinetics of a K_2CO_3 composite are investigated under pure water vapor conditions. Moreover the effect of CO_2 emissions of K_2CO_3 in a closed system is studied.

2. Materials

Within the framework of the CREATE project [30] a K_2CO_3 composite particle has been developed allowing low cost and industrial large scale production. For reactor scale applications K_2CO_3 cannot be used in its powder form, as the bed permeability would be too low. Since the permeability is a function of the particle radius, particles are prepared in the range of 1–5 mm [31] For material characterization in this research the material is sieved in a smaller fraction with a size of 1.4–2.0 mm (50 g sample size).

The composite material was optimized according to the following criteria, in order of importance: pT line, degassing, energy density, kinetics, mechanical stability and thermal conductivity. After an extensive analysis of different composites, including several production routes, optimization of production parameters and selection of material additives, the most optimal composite turned out to be a compacted granule with a binder material. The granules are produced by Caldic B.V. (Caldic Ingredients Deutschland GmbH, Düsseldorf). The production process consists of grinding, mixing, compacting, granulating and sieving [31].

The base material is hydrous, meaning that it is completely hydrated, for K_2CO_3 a 1.5 hydrate. This hydrous state is necessary for the application since the phase transition of a salt hydrate is associated with a volume change. Whereby the volume change is caused by the incorporation of water in the crystal lattice of the salt. For K_2CO_3, from anhydrous to hydrous this volume change is 11.5%. Due to this it is important that the material is fully hydrated upon filling the heat exchanger, otherwise this volume increase can damage the heat exchanger during hydration.

The compacted bars can be seen in Fig. 3a, and the granulated end product can be seen on 3b. A large scale production costs evaluation, including capital expenditures and operating expenses, assuming a production volume 1000 units of 2.5 m^3 concludes that the final composite can be produced at 1.4 €/kg, according to H. van der Meer (personal communication, March 2018). Concluding that the raw material price accounts about 90% of the composite cost and thus a cost efficient production route is developed [31].

The bulk energy storage density (ESD) of the composite is proportional to the ESD of pure crystalline $K_2CO_3 \cdot 1.5H_2O$ which has an ESD of 1.30 GJ/m^3 [28]:

$$ESD_{comp} = \frac{\rho_{comp}}{\rho_{crys}} \cdot ESD_{crys} \quad (2)$$

in which ρ [kg/m^3] is the density of either the composite or crystal, for $K_2CO_3 \cdot 1.5H_2O$ the crystal density is 2.18 g/mL [4]. Full conversion (i.e. cyclic full loading and unloading of the TCM) was possible in thermogravimetric measurements, see Fig. 4. Which allows the use of equation (2) for calculations of the bulk energy density.

The bulk energy density of approximately 150 g material was measured inside a cylinder of 250 mL with a diameter of 4 cm. The density was determined by measuring the volume increase of isopropanol after the addition of the composite grains. The maximum

(a) (b)

Fig. 3. a): compacted bars of the 97% K_2CO_3 base material and binder. b): bars granulated into final composite granules.

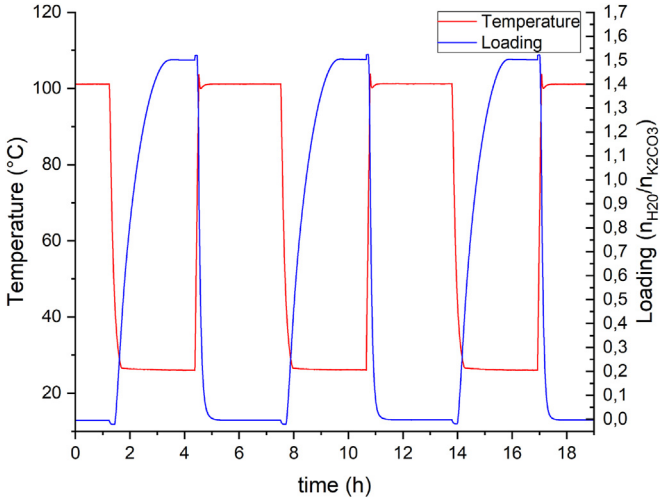

Fig. 4. Cyclic loading of the K_2CO_3 composite at 12 mbar as measured with TGA. The red line indicates the material temperature and the blue line the loading. Full loading of 1.5 mol H_2O/mol K_2CO_3 is reached. (For interpretation of the references to color in this figure legend, the reader is referred to the Web version of this article.)

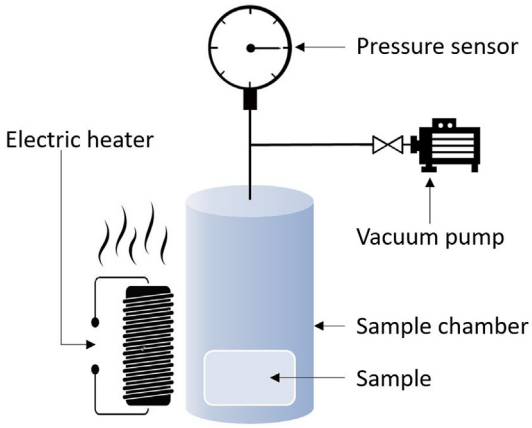

Fig. 5. Schematic illustration of the pT setup. The sample is placed in the sample chamber, which is evacuated using a vacuum pump. The chamber temperature is controlled with an electric heater, the chamber pressure is measured using a pressure transmitter. The setup is thermal insulated and heated to avoid internal condensation.

ESD obtained was 0.84 GJ/m^3, which was achieved after tapping the material using a vortex shaker. The tapping resulted in an energy density increase of 20% [31].

3. Methods

In this section the methods and in-house developed setups are described that are used to obtain thermodynamic and kinetic data for the characterization of the composite under pure water vapor conditions. As the focus of this work was on experimental characterization, use has been made on existing theory. It has to be remarked that the nature of the transport processes is such that there was no need for developing new theory. Therefore the theory used in this work is building on existing theory as presented by [13].

3.1. Phase diagrams: equilibrium hydration line - pT line

Fig. 5 shows the experimental setup which is used to determine the phase diagram of K_2CO_3. This is done by measuring equilibrium pressure-temperature points of the hydration/dehydration transition. Note that the water vapor pressure equals the total pressure. The absolute water vapor pressure is measured under vacuum conditions. The setup consists of a temperature controlled sample chamber in which the material temperature is controlled. The heat is generated with an electric resistance band heater and the temperature is controlled with an Eurotherm ® 2216e PID controller. The temperature range is from room temperature till 140 °C with an accuracy of ± 1 °C. The pressure inside the setup is measured with a KOBOLD ® PAS pressure transmitter. In the calibrated range the accuracy of the sensor is 0.15 mbar. The complete setup is thermal insulated and heated to avoid internal condensation. The heating is done with an electrical resistance wire which is electrically insulated by a braided fibreglass cable sleeve. The thermal insulation is done with mineral wool tube insulation. The procedure to measure a pT line is as follows. A constant temperature is applied until the equilibrium pressure is reached. Subsequently the temperature is increased stepwise and the next equilibrium pressure is determined. From these data points the phase diagram is constructed.

3.2. pT-mass setup

In this section the setup and methods are described, which are used to measure; kinetics, metastable behavior, the amount of impurities in the base material, the effect of NCG in a closed reactor system and the cyclic performance of K_2CO_3 in a closed reactor system. The setup is a small scale reactor consisting of two

temperature controlled vessels in which the mass of one vessel can be measured as function of time.

3.2.1. Kinetics

To study the hydration/dehydration kinetics, a new setup has been constructed called the pT-mass setup. This pT-mass setup is shown in Fig. 6, where the mass of vessel 2 is measured over time.

Vessel 1 has a volume of 108 mL and can be temperature controlled between −20 and 80 °C using a thermostatic bath with an accuracy of 0.1 °C (LAUDA ® RE 415 silver). Vessel 2 has a volume of 224 mL and can be temperature controlled between room temperature and 200 °C using an electrical resistance heater with a power of 30 W. The temperature sensor, of the heater of vessel 2, is located on the bottom of the vessel which can cause a small temperature deviation inside the sample as the heat conductivity of salt hydrates are generally low (0.2–1 W/mK). To measure the actual sample temperature two thermocouples are inserted in vessel 2. Thermocouples are type K and data acquisition is done with a National instruments™ NI 9211 thermocouple input module. To reduce the temperature gradient in the material vessel 2 contains an integrated heat exchanger.

The stainless steel tubing to connect both vessels is partly flexible to mechanically decouple the vessels and measure the mass variations. The tubing is heated above 80 °C to avoid internal condensation. The tubing internal diameter is 4 mm with a reduction to 2 mm at the valve position, the internal diameter of the flexible tubing is 15 mm. The total length of the tubing is 0.8 m with 0.5 m of flexible tubing, the pressure drop is less than 10 Pa. Vessel 2 is placed on a balance with an accuracy of 0.01 g (Mettler Toledo ® XPE6000). Above vessel 1, a pressure sensor is located with and accuracy of 0.2 mbar in the range of 0–200 mbar (Kobold ® PAS).

3.2.2. Metastable zone

The boundaries of the metastable zone of the K_2CO_3 composite are determined by varying the temperature at isobaric water vapor conditions. The water vapor pressure is kept constant by controlling the temperature of vessel 1 in Fig. 6. The horizontal dashed line in Fig. 7 indicates this isobaric condition. The initial hydration state is completely anhydrous, which is prepared ex-situ in an oven at 130 °C for at least 48 h. Before the start of each measurement the dehydration is prolonged in-situ to remove all water that has been absorbed during sample handling. In-situ dehydration conditions are 130 °C under continuous vacuum pump down. The metastable zone boundary is determined as the onset point of hydration. The onset point can be determined from the both the material temperature and the mass of the sample, since the hydration is associated with both energy release and mass uptake. In this study we have used the temperature as it is more sensitive to sudden changes in the reaction rate.

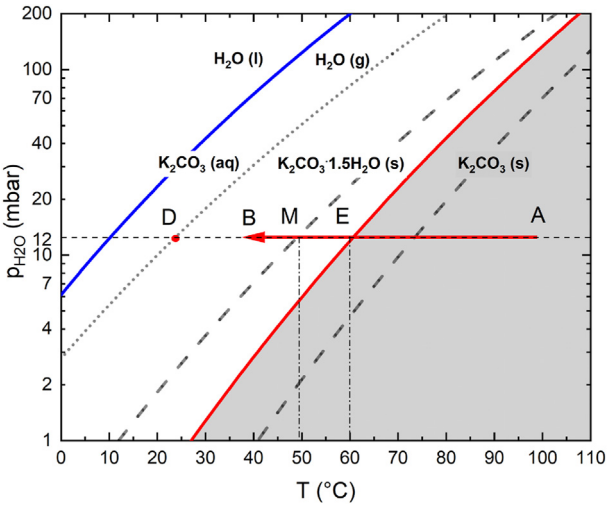

Fig. 7. Isobaric measurement to determine the onset of hydration. The upper solid line (blue) indicates the water line. Lower solid line (red) indicates the K_2CO_3 phase transition line, the area under the curve (gray colored) is the anhydrous phase, above is the hydrous phase. The dotted line is the deliquescence line. Measurements start in point A, then the temperature is lowered with a constant cooling rate towards point B. Point D indicates the deliquescence onset point, M the hydration onset point and E the equilibrium point. (For interpretation of the references to color in this figure legend, the reader is referred to the Web version of this article.)

The measurement protocol for a single onset point is illustrated in Fig. 7. A measurement starts in point A, where the material is anhydrous, the material is cooled down in the direction of point B with a constant cooling rate. Without metastable behavior one would expect hydration when the temperature crosses point E: the

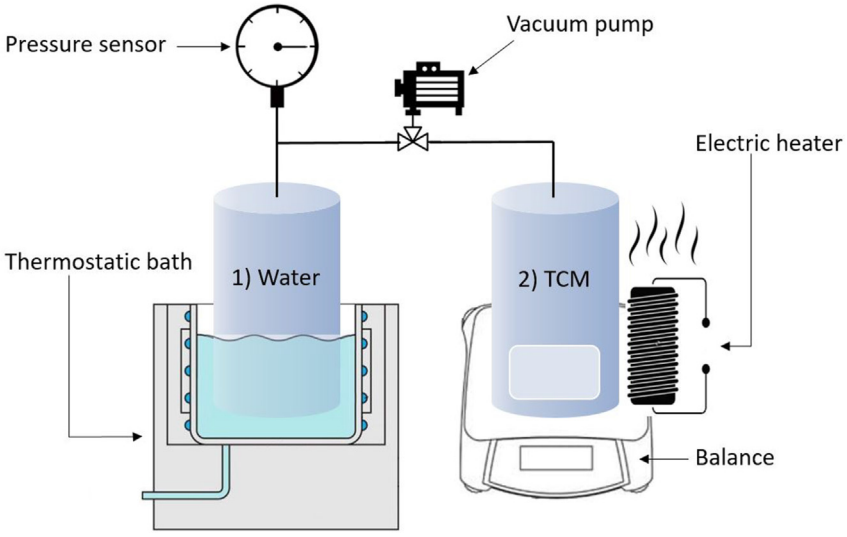

Fig. 6. Schematic illustration of the pT-mass setup. Vessel 1 contains water and acts as evaporator/condenser, vessel 2 contains the TCM. The mass of vessel 2 is measured so the hydration state and kinetics can be measured. Both vessels are temperature controlled and the entire setup is heated to avoid internal condensation in the tubing.

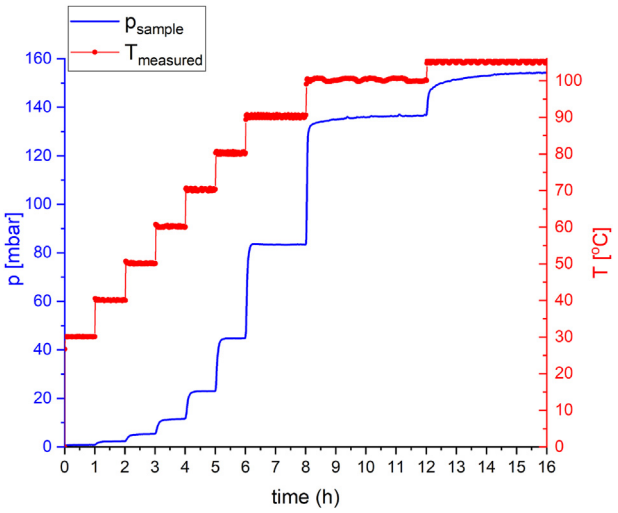

Fig. 8. Typical pT measurement with the sample pressure on the left y-axis (blue solid line) and the sample temperature (red dotted line) on the right y-axis as a function of time. The equilibrium line is obtained from the equilibrium pressure at the end of each temperature step. (For interpretation of the references to color in this figure legend, the reader is referred to the Web version of this article.)

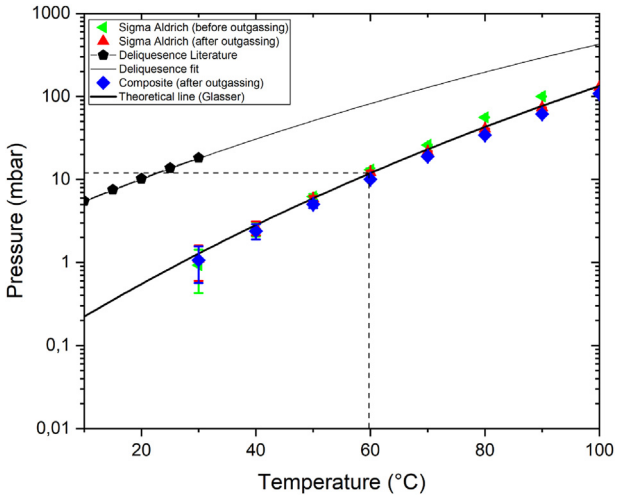

Fig. 9. Equilibrium phase transition lines as measured with the pT-setup. Triangle markers indicate ACS grade K_2CO_3 from Sigma Aldrich, before and after degassing (green and red respectively). The diamond markers (blue) indicate the CREATE composite, which is in agreement with Glasser [8]. The upper solid line indicates the deliquescence line. (For interpretation of the references to color in this figure legend, the reader is referred to the Web version of this article.)

equilibrium phase transition point. When metastable behavior is the same under pure water vapor conditions as under atmospheric conditions, the onset point of hydration is expected around the metastable point M [10]. If the material is cooled further from point B towards point D the deliquescence onset point can be determined.

3.2.3. Degassing

By a degassing step the $KHCO_3$ impurities can be removed and the amount of impurities can be determined. This is done as follows; the material in vessel 2 (Fig. 6) is heated to a temperature of 120 °C, the crystal water of K_2CO_3 will be released and condensed in vessel 1, $KHCO_3$ impurities will decompose into K_2CO_3(s), CO_2 (g) and H_2O (g) [28]. H_2O (g) will condense in vessel 1 but CO_2 (g) will not condense and remain as non-condensable gas (NCG) in the system. The total pressure in the system is the sum of the partial pressure of water and the partial pressure of CO_2; since the partial pressure of water is known from the temperature of vessel 1, the partial pressure of CO_2 can be determined. Since the free volume of the setup is known the amount of impurities in the base material can be determined using the ideal gas law:

$$n = \frac{PV}{RT} \tag{3}$$

With n [mol] the amount of material, P [Pa] the pressure, R [J/K/mol] the gas constant, T [K] the temperature and V [m^3] the free volume in the setup.

3.2.4. Cyclability and the role non-condensable-gasses

To study the cyclic performance of the K_2CO_3 composite, two types of experiments have been performed. Both experiments are performed at constant water vapor pressure of 12 mbar (10 °C at the evaporator/condenser in vessel 1, Fig. 6). The material is cycled by varying the temperature of vessel 2 between 40 °C and 90 °C.

In the first experiment we allow for one source of NCG: gasses dissolved in water at the evaporator/condenser. Demi-water is prepared with a Mili-Q ®. Before cycling the demi-water is not further pre-treated to remove NCG dissolved in water. The K_2CO_3 composite material is degassed ex-situ to remove all bi-carbonate and evacuated in situ for 30 min to remove adsorbed NCG on the surface. The leakage rate of the setup has been determined and was an order of magnitude lower to be a source of NCG affecting the measurements. In this experiment the only sources of NCG are thus the gasses dissolved in water.

In the second experiment the material is hydrated ex-situ in a vacuum oven at 50 °C to avoid bicarbonate formation, the water source is a saturated magnesium chloride solution (RH 33%). Before hydration the material was degassed at 120 °C for t > 48 h. In this experiment vessel 1 in Fig. 6 is empty and vessel 2 is filled with the hydrated material. Therefore the only water introduced in the system is crystal water. The material is now cycled to investigated the cyclic stability of K_2CO_3 when all sources of non-condensable gasses are eliminated.

4. Results & discussion

4.1. Phase diagram: pT line

With the pT-setup the phase transitions lines of various K_2CO_3 powders and composites are measured. A typical measurement for the K_2CO_3 composite granules is shown in Fig. 8. On the left and right y-axes, the water vapor pressure and the sample temperature are shown respectively. First the system is equilibrated at the starting temperature. When the vapor pressure reaches its equilibrium value the temperature is increased stepwise, after each temperature step the pressure adopts a new equilibrium value that depends on the set temperature.

The obtained equilibrium phase lines are shown in Fig. 9. Here it can be seen that the K_2CO_3 composite (solid blue diamonds) phase line does not deviate from the line of pure K_2CO_3 as reported by Glasser [8]. Moreover it corresponds to the equilibrium line of pure K_2CO_3 of ACS grade from Sigma Aldrich (triangles markers). From this is concluded that the binder material does not influence the phase transition of K_2CO_3.

By the verification of the pT line (and thus the phase diagram) with literature data as reported by Ref. [8], it is confirmed that the K_2CO_3 based composite operates as desired. Meaning that a water vapor pressure of 12 mbar could generate a hydration temperature,

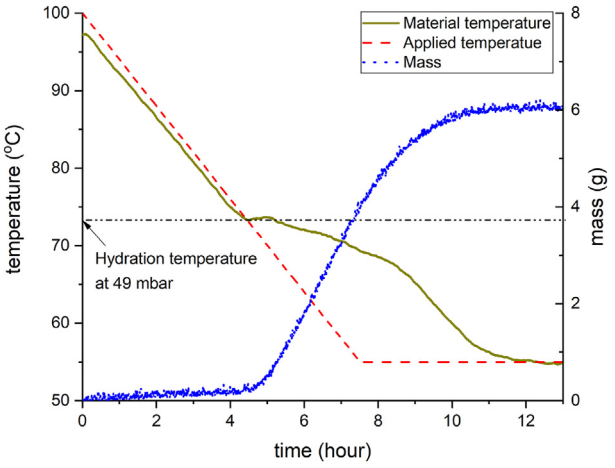

Fig. 10. Typical pT-mass measurement to determine the hydration onset temperature at a water vapor pressure of 49 mbar with a cooling rate of 0.1 K/min. Temperatures are given by the left y-axis and the sample mass on the right y-axis. The dashed red line and the yellow solid line are the set temperature and the actual measured material temperature respectively. The blue line represent the mass increase of the sample. (For interpretation of the references to color in this figure legend, the reader is referred to the Web version of this article.)

T_{hy} > 50 °C and a dehydration temperature, T_{deh} < 120 °C, as required for a residential application [4].

4.2. Impurity removal by degassing

Looking at lab grade K_2CO_3 from Sigma Aldrich, triangular markers, the effect of impurities can already be seen on the pT-equilibrium line, see Fig. 10. The left pointing triangles are measured pressures before a degassing procedure and the upper pointing triangles are equilibrium pressures measured after a degassing procedure and partial re-hydration. The equilibrium pressure of Sigma Aldrich material before degassing is higher than after degassing due to the partial CO_2 pressure originating from the decomposition of bicarbonate impurities. The decomposition becomes notable at temperatures above 50 °C, where the observed pressure exceeds the expected equilibrium pressure. For the composite base material, K_2CO_3 different suppliers are verified on the CO_2 decomposition. Typical results are shown in Table 1.

From Table 1 it can be seen that the hydrous base material contains impurities in the same order as the anhydrous base material. Further, it demonstrates that degassing effectively removes the impurities in both composites from hydrous and anhydrous base material.

4.3. Metastable zone

To study the metastable zone under pure water vapor conditions, the onset points for hydration are measured with the pT-mass setup and compared with previously published data obtained under atmospheric conditions [10].

A typical experiment to determine the hydration onset point at 49 mbar is shown in Fig. 10. The left y-axis indicates the temperature and the right y-axis indicates the sample mass. The red dashed line indicates the applied temperature on the sample chamber, the yellow solid line represents the material temperature. The mass increase is plotted with the solid blue line. The onset temperature can be determined as the inflection point of the material temperature, the corresponding temperature is indicated with the horizontal dashed-dotted line. After this point also a significant mass increase is observed, corresponding to the hydration reaction.

Table 1
Impurities for different composite base materials (* as detectable in our setup).

Base material	Impurities		Impurities after degassing
	[mbar/gram]	[mol/gram]	[mol/gram]
Anhydrous	0.38	4.3	0*
Hydrous	0.32	3.6	0*

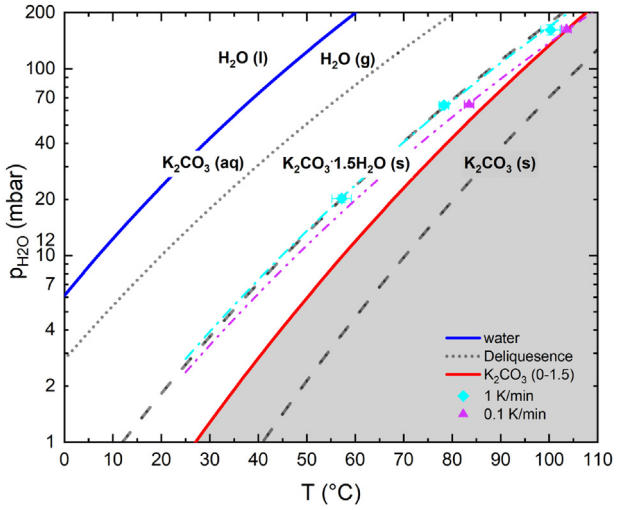

Fig. 11. The metastable zone boundary under pure water vapor conditions as measured with the pT-mass setup. Dashed lines are the metastable zone boundaries for hydration and dehydration, as measured under atmospheric conditions for pure K_2CO_3[10]. The light blue squares indicate hydration onset points for a cooling rate at 1 K/min and the purple triangle markers indicate measurements at a rate of 0.1 K/min material. (For interpretation of the references to color in this figure legend, the reader is referred to the Web version of this article.)

This type of measurement is repeated for different vapor pressures to construct the boundary of the meta-stable zone as shown in Fig. 11. On the y-axis the water vapor pressure is shown and on the x-axis the temperature. The red solid line represents the equilibrium line of K_2CO_3, the dashed line on both sides of the equilibrium line represent the metastable zone boundary as found under atmospheric conditions [10]. The dotted line is the deliquescence line of K_2CO_3 and the blue solid line is the water line. The light blue squares are hydration onsets point for a cooling rate of 1 K/min, the light blue dashed-dotted line is an extrapolation of the data points. The purple triangle markers and dashed-dotted line represent the hydration onset point and extrapolation respectively of the measurements at a cooling rate of 0.1 K/min.

The first experiments were done at a cooling rate of 1 K/min. In Fig. 11, the onset points for hydration in vacuum (light blue squares) are plotted as an overlay on the metastable line extrapolation (dashed lines) as found by Sögütoglu et al. [10] for atmospheric conditions. The observed onset points clearly coincide with the metastable line as observed for atmospheric conditions. This verifies the existence of a metastable zone under pure water vapor conditions. It has to be stressed that our measurements cover a much wider range in terms of vapor pressure, from 20 mbar vapor pressure up to 165 mbar, than presented in the previous study under atmospheric conditions. Therefore, our measurements justify the extrapolation done by Ref. [10].

In the second set of experiments, a lower cooling rate of 0.1 K/min has been applied. These experiments were only performed at higher vapor pressures: 65 and 165 mbar. The corresponding onset

points are plotted as the purple triangles in Fig. 11. It seems that with increasing vapor pressure these onset points are much closer to the equilibrium line, indicating that the induction times for nucleation are much shorter for hydration under vacuum conditions. It seems that, especially at higher vapor pressure (higher temperature), the metastable zone is much more narrow than expected based on the previous studies [10]. More measurements at different cooling rates, especially at lower vapor pressures, have to be performed to draw definitive conclusions. This could either be a consequence of using pure water vapor conditions instead of working under atmospheric conditions, or the higher pressures and temperatures used in our experiment.

As a side remark it should be mentioned that the material investigated under atmospheric conditions was pure K_2CO_3 powder and the material studied in this paper is a K_2CO_3 composite. Although we do not expect an influence of the added binder this has to be verified by measuring the onset temperatures of the composite also under atmospheric conditions.

4.4. Cyclability and non-condensable-gasses

Now that it is shown in section 3.2.3, that $KHCO_3$ impurities can be removed by a degassing step, we focus on the effect of other sources of NCG in general and gasses dissolved in the water in particular. Two experiments have been performed. In the first experiment all NCG have been removed except from the gasses dissolved in water. In the second experiment the only water present is the bound crystal water of the salt hydrate and therefore the water reservoir cannot act as a source of NCG.

In the first cycling experiment untreated demi-water is put in the evaporator/condenser and anhydrous K_2CO_3 in the other vessel. Note that all water present at the start is located in the evaporator/condenser. Results are shown in Fig. 12. In the upper, middle and lower graph the material temperature, water vapor pressure and mass are shown respectively. Subsequent cycles are indicated by the arrow. Clearly the hydration rate decreases over cycling. Moreover water vapor pressure increases during the dehydration phase, which indicates that the amount of NCG increases during cycling.

To determine if these gasses can originate from the water vessel, first the amount of dissolved gasses has been determined by using Henry's law, see equation Appendix A. It is assumed that the gasses are initially dissolved in demi-water under atmospheric pressure. The following gasses are taken into account, N_2, O_2 and CO_2. With the corresponding Henry's solubility constants ($H = N26.4 \cdot 10^{-6}$, $H = O21.3 \cdot 10^{-5}$ and $H = CO23.3 \cdot 10^{-4}$ mol/m^3/Pa) [32], a pressure increase of 2.6 mbar is estimated. For details see A. By Donkers et al. it is already shown that an amount of inert gasses with a pressure of 1 mbar can significantly reduce the evaporation and condensation rates of water [21]. Therefore it is plausible that the decrease in hydration rate is due to the release of gasses dissolved in water.

Clearly the NCG coming from water block the vapor transport. The NCG are carried by the vapor flow from one vessel to the other. The water will condense or be absorbed but the NCG not. The NCG then form a layer above the surface reducing the water vapor flow.

Then the initial build-up in pressure is caused by the blocking of vapor flow from TCM to condenser (from vessel 2 to vessel 1 in Fig. 6). Finally the pressure will go down as the water diffuses trough the layer of NCG and condenses. If condensation would be blocked completely during hydration the pressure would approach the equilibrium pressure of K_2CO_3 at 90 °C (77 mbar). The reduction in condensation rate shows that more NCG is released from the water with each subsequent cycle.

Other sources of NCG cannot explain this significant decrease in reduction of dehydration rate. The inleak of NCG (air) is an order of magnitude lower to have an effect on the hydration rate.

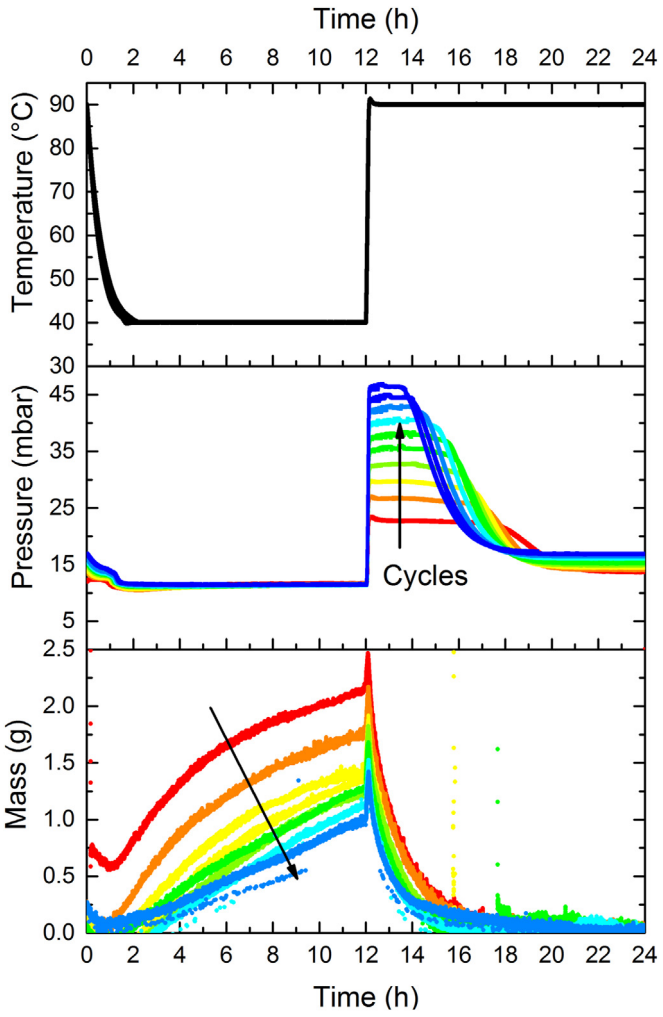

Fig. 12. Cyclic hydration experiment. Subsequent cycles are indicated by the direction of the arrow, where red marks the first cycle and blue the last cycle. Top: temperature as function of time. Middle: Pressure as function time where it can be seen that the condensation rate decreases over each cycle. Bottom: Mass as function of time, decreasing hydration rate due to NCG coming from the water source. (For interpretation of the references to color in this figure legend, the reader is referred to the Web version of this article.)

To further verify this, a second experiment is performed. Here we start without water in the evaporator (vessel 1 Fig. 6). The start material is now degassed and hydrated ($K_2CO_3 \cdot 1.5H_2O$). The only water present in the system is thus crystal water and thereby all sources of NCG are removed, the results are shown in Fig. 13. The first step is a dehydration step. In the middle graph, pressure as function of time, it can be seen that during dehydration there is hardly any pressure build-up compared to Fig. 12. The slight pressure build-up can be attributed to leakage from the ambient. In the lower graph of Fig. 13, it is shown that all dehydration and hydration cycles have the same rate and are stable over 14 cycles.

Compared to the significant decrease in condensation rate in experiment 1 (Fig. 12) it can be concluded that, the in water dissolved gasses, in the evaporator/condenser vessel have a significant effect on the performance of a closed system. And that pretreatment of water is of crucial importance for stable performance of a closed system. More important, it can be seen in Fig. 13 that if given that $KHCO_3$ impurities have been removed by a heat treatment, K_2CO_3 can be cycled without a loss of performance.

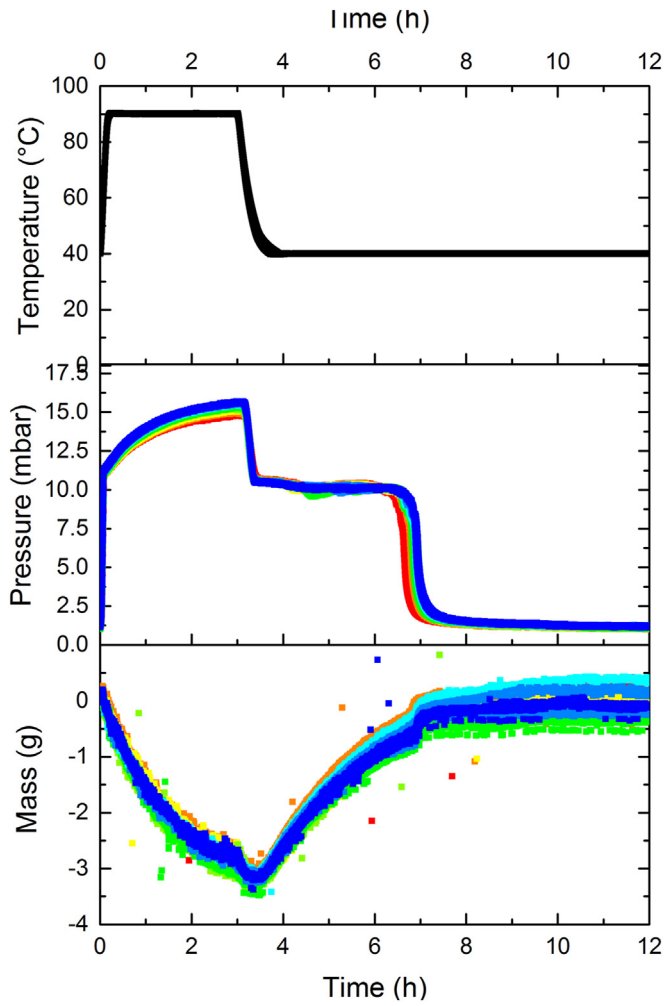

Fig. 13. Cyclic experiment with hydrated start material. The different colors denote different cycles. Top: temperature as function of time. Middle: Pressure as function time, slight variation in pressure. Bottom: Mass as function of time, with some variation all cycles overlap in hydration rate. (For interpretation of the references to color in this figure legend, the reader is referred to the Web version of this article.)

5. Conclusions

For the first time, a novel selected TCM material, a K_2CO_3 composite, is investigated on its suitability for a closed reactor system, operating under pure water vapor conditions. The thermodynamics, kinetics and cyclability have been studied under reactor conditions.

For a large scale application the material cannot be used in the form of a powder, due to the low permeability of a powder bed. To that extend particles have been produced in a range of 1–5 mm. It is shown that a state of the art K_2CO_3 composite granular material can be produced [31]. The equilibrium and kinetic behavior of the composite is investigated under vacuum conditions as current data for K_2CO_3 was only available for atmospheric hydration/dehydration.

First of all the thermodynamics was verified by measuring the phase diagram based on pressure-temperature equilibrium points. It can be concluded that the hydration transition of K_2CO_3 in pure water vapor coincides with data reported for atmospheric conditions (lab grade powder and composite) and can be used in view of the intended temperature window.

Our measurements indicate that the metastable behavior found under atmospheric conditions is also present under pure water vapor conditions. In the metastable zone nucleation limits the hydration rate, compared to atmospheric conditions there are indications that the induction times for nucleation are shorter in vacuum conditions. A heating/cooling rate dependency has been found under vacuum conditions, which has not been observed in atmospheric conditions. Current work focuses on the collection of detailed induction time data inside the metastable zone to gain more insight in the nucleation process.

The implications of a metastable zone are that the temperature operating window is limited from the equilibrium line towards the metastable line (MZW of 13 °C). Current work focuses on the introduction of nucleation promoters to enhance nucleation and reduce the meta-stable zone width and to enhance kinetics in general.

In a closed system non-condensable gasses (NCG) can have a significant effect on the hydration/dehydration rates. NCG can be released by the material if it contains $KHCO_3$ impurities. If $KHCO_3$ impurities are present in the K_2CO_3 composite the equilibrium pressures measured are higher due to CO_2 degassing, it is shown that these impurities can effectively be removed by a degassing step, this holds for all investigated base materials.

Finally, cyclability studies of K_2CO_3 show that except from purifying the material it is critical to remove dissolved gasses from water in the evaporator/condenser vessel. If water is well treated the K_2CO_3 composite can by cycled in a closed reactor system without compromising performance over at least 14 cycles.

Our study shows that K_2CO_3 composites are suitable for usage in a closed reactor system operating under pure water vapor pressure.

CRediT authorship contribution statement

Jelle Houben: Writing - original draft, Writing - review & editing, Conceptualization, Methodology, Investigation. **Leyla Sögütoglu:** Conceptualization, Methodology. **Pim Donkers:** Conceptualization, Methodology, Validation, Investigation. **Henk Huinink:** Supervision, Project administration, Funding acquisition, Conceptualization, Validation, Writing - review & editing. **Olaf Adan:** Supervision, Project administration, Funding acquisition.

Declaration of competing interest

The authors declare that they have no known competing financial interests or personal relationships that could have appeared to influence the work reported in this paper.

Acknowledgements

This project has received funding from the European Union's Horizon 2020 research and innovation program under grant agreement No 680450. This work reflects only the authors view. The European Commission is not responsible for any use that may be made from this information. The authors thank Henry van der Meer for supplying the composite materials used in this work and Hans Dalderop and Jef Noijen for their technical support.

Appendix A. Pressure build-up using Henry's law

To estimate the pressure build-up in the setup due to the release of NCG dissolved in water, the maximum amount of NCG dissolved in the water is estimated. The amount of dissolved gas is proportional to the partial pressure of a gas. The demi-water used in the experiments is prepared at atmospheric pressure. Therefore the partial pressures of the gasses in air at atmospheric pressure are taken and it is assumed that the gasses are dissolved up to the

equilibrium concentration. With Henry's law one can calculate the concentration of a dissolved gas in the liquid water phase. The concentration of a dissolved gasses can be expressed as:

$$c_a = H_{cp} \cdot p \tag{A.1}$$

here, c_a [mol/m^3] is the concentration of the constituent in the aqueous phase, H_{cp} [mol/m^3/Pa] the Henry's law constant, and p [Pa] the partial pressure of the constituent in the gas phase under equilibrium conditions. The following gasses are taken into account, N_2, O_2 and CO_2. The corresponding Henry's solubility constants are given in Table A.2, together with the partial pressure of the gasses in air at atmospheric conditions [32].

Table A.2
Overview of Henry's law solubility constants and the partial pressure of the gasses taken into account [32]. With equation Appendix A, the concentrations are determined as shown in the column on the right.

Gas	Solubility constant [mol m^{-3} Pa-1]	Partial pressure of gas [Pa]	Concentration [mol m^{-3}]
N_2	$6.4 \cdot 10^{-6}$	$7.9 \cdot 10^{4}$	$5.1 \cdot 10^{-1}$
O2	$1.3 \cdot 10^{-5}$	$2.1 \cdot 10^{4}$	$2.8 \cdot 10^{-1}$
CO_2	$3.3 \cdot 10^{-4}$	$4.2 \cdot 10^{1}$	$1.4 \cdot 10^{-2}$

In the experiment the evaporator is filled with 30 mL demi-water. With the assumption that all gasses behave as an ideal gas the total amount of gas can be determined by:

$$n_{gas} = (C_{N2} + C_{O2} + C_{CO2}) \cdot V_{water} \tag{A.2}$$

where n_{gas} [mol] is the amount of gas and V_{water} [m^3] the water volume. With a water volume of 30 mL a maximum of $2.4 \cdot 10^{-5}$ mol of gasses can be dissolved. Since the volume of the setup is known, the pressure build-up can be determined by using the ideal gas law. The volume of the setup is 332 mL, the material volume 25 mL and the water volume 30 mL. This results in a free volume of 280 mL. With $2.4 \cdot 10^{-5}$ mol initially dissolved gasses this will give a potential gas pressure of 2.6 mbar.

References

[1] European Commission, Roadmap 2050, Policy (2012) 1-9, ISSN 14710080, doi: 10.2833/10759, URL http://www.roadmap2050.eu/. doi:10.2833/10759. arXiv:ISBN 978-92-79-21798-2.

[2] K. Edem N'tsoukpoe, T. Schmidt, H.U. Rammelberg, B.A. Watts, W.K.L. Ruck, A Systematic Multi-step Screening of Numerous Salt Hydrates for Low Temperature Thermochemical Energy Storage, 2014, https://doi.org/10.1016/j.apenergy.2014.02.053.

[3] L. Itard, F. Meijer, Towards a Sustainable Northern European Housing Stock Figures, facts and future Delft Centre for Sustainable Urban Areas, ISBN 209.

[4] P.A. Donkers, L.C. Sögütoglu, H.P. Huinink, H.R. Fischer, O.C. Adan, A review of salt hydrates for seasonal heat storage in domestic applications, Appl. Energy 199 (2017) 45–68, https://doi.org/10.1016/j.apenergy.2017.04.080.

[5] A. Fopah Lele, F. Kuznik, H.U. Rammelberg, T. Schmidt, W.K. Ruck, Thermal decomposition kinetic of salt hydrates for heat storage systems, Appl. Energy 154 (2015) 447–458, https://doi.org/10.1016/j.apenergy.2015.02.011.

[6] T. Kousksou, P. Bruel, A. Jamil, T. El Rhafiki, Y. Zeraouli, Energy Storage: Applications and Challenges, 2014, https://doi.org/10.1016/j.solmat.2013.08.015.

[7] I. LTS Research Laboratories, International, Tech. Rep., LTS Research Laboratories, Inc., Orangeburg, 2015.URL https://www.ltschem.com/msds/K2CO3.pdf.

[8] L. Glasser, Thermodynamics of inorganic hydration and of humidity control, with an extensive database of salt hydrate pairs, J. Chem. Eng. Data 59 (2) (2014) 526–530. http://pubs.acs.org/doi/abs/10.1021/je401077x doi:10.1021/je401077x.

[9] L. Greenspan, Humidity Fixed Points of Binary Saturated Aqueous Solutions, Tech. Rep, vol. 1, Institute for Basic Standards, National Bureau of Standards, Washington, D. C., 1977.

[10] L.C. Sögütoglu, M. Steiger, J. Houben, D. Biemans, H.R. Fischer, P. Donkers, H. Huinink, O.C. Adan, Understanding the hydration process of salts: the impact of a nucleation barrier, Cryst. Growth Des. 19 (4) (2019) 2279–2288, https://doi.org/10.1021/acs.cgd.8b01908.

[11] C. Geelen, L. Krosse, P. Sterrenburg, E.-J. Bakker, N. Sijpheer, Nederlandse Organisatie voor toegepast-natuurwetenschappelijk onderzoek / Netherlands Organisation for Applied Scientific Research, Tech. Rep., URL www.mep.tno.nl, 2003.

[12] V.I. Kalikmanov, Nucleation Theory vol. 860 (2013), https://doi.org/10.1007/978-90-481-3643-8.arXiv:1211.6245.

[13] L. Scapino, H.A. Zondag, J. Van Bael, J. Diriken, C.C. Rindt, Energy Density and Storage Capacity Cost Comparison of Conceptual Solid and Liquid Sorption Seasonal Heat Storage Systems for Low-Temperature Space Heating, Renewable and Sustainable Energy Reviews, 2017, https://doi.org/10.1016/j.rser.2017.03.101.

[14] D. Vanhoudt, B. Claessens, F. De Ridder, G. Reynders, V.R. Cuypers, H. Oversloot, C. Finck, C.V. Soest, A. De Jong, E. Henquet, H. Van 't Spijker, F. Koene, R. De Boer, S. Smeding, H. Zondag, D3.2 Report on a Combination of Thermal Storage Techniques and Components, 2015.

[15] B. Michel, P. Neveu, N. Mazet, Comparison of Closed and Open Thermochemical Processes, for Long-Term Thermal Energy Storage Applications to Cite This Version : HAL Id : Hal-01025210 Storage Applications Abstract, 2014.

[16] U. Stritih, U. Mlakar, Technologies for seasonal solar energy storage in buildings, in: Advancements in Energy Storage Technologies, InTech, 2018, https://doi.org/10.5772/intechopen.74404.

[17] A.J. De Jong, L. Van Vliet, C. Hoegaerts, M. Roelands, R. Cuypers, Thermochemical heat storage - from reaction storage density to system storage density, in: Energy Procedia, 2016, https://doi.org/10.1016/j.egypro.2016.06.187.

[18] B. Fumey, R. Weber, L. Baldini, Sorption based long-term thermal energy storage â€“ Process classification and analysis of performance limitations: a review, Renew. Sustain. Energy Rev. 111 (2019) 57–74, https://doi.org/10.1016/j.rser.2019.05.006.

[19] T. Yan, R.Z. Wang, T.X. Li, L.W. Wang, I.T. Fred, A Review of Promising Candidate Reactions for Chemical Heat Storage, 2015, https://doi.org/10.1016/j.rser.2014.11.015.

[20] R. De Boer, W.G. Haije, J.B.J. Veldhuis, S.F. Smeding, Solid sorption cooling with integrated thermal storage: the SWEAT prototype. https://www.ecn.nl/docs/library/report/2004/rx04080.pdf, 2004.

[21] P. Donkers, K. Gao, J. Houben, H. Huinink, B. Erich, O. Adan, Effect of non-condensable gasses on the performance of a vacuum thermochemical reactor, Energies 13 (2020), https://doi.org/10.3390/en13020362.

[22] R. Weber, V. Dorer, Long-term heat storage with NaOH, Vacuum 82 (2008) 708–716, https://doi.org/10.1016/j.vacuum.2007.10.018.

[23] B. Fumey, R. Weber, P. Gantenbein, X. Daguenet-Frick, S. Stoller, R. Fricker, V. Dorer, Operation results of a closed sorption heat storage prototype, in: Energy Procedia, 2015, https://doi.org/10.1016/j.egypro.2015.07.698.

[24] H.U. Rammelberg, T. Schmidt, W. Ruck, Hydration and dehydration of salt hydrates and hydroxides for thermal energy storage - kinetics and energy release, in: Energy Procedia, vol. 30, Elsevier Ltd, 2012, pp. 362–369, https://doi.org/10.1016/j.egypro.2012.11.043.

[25] O. Opel, H.U. Rammelberg, M. Gérard, W. Ruck, Thermochemical storage materials research-TGA/DSC-hydration studies, 1st International Conference for Sustainable Energy Storage (2011).

[26] M. Roelands, R. Cuypers, K.D. Kruit, H. Oversloot, A.J. De Jong, W. Duvalois, L. Van Vliet, C. Hoegaerts, Preparation & characterization of sodium sulfide hydrates for application in thermochemical storage systems, Energy Procedia 70 (2015) 257–266, https://doi.org/10.1016/j.egypro.2015.02.122, 0.

[27] A.J. De Jong, F. Trausel, C. Finck, L. Van Vliet, R. Cuypers, Thermochemical heat storage - system design issues, Energy Procedia 48 (48) (2014) 309–319, https://doi.org/10.1016/j.egypro.2014.02.036.

[28] L.C. Sögütoglu, P.A. Donkers, H.R. Fischer, H.P. Huinink, O.C. Adan, In-depth investigation of thermochemical performance in a heat battery: cyclic analysis of K CO , MgCl and Na S, Appl. Energy 215 (2018) 159–173, https://doi.org/10.1016/j.apenergy.2018.01.083. 2322.

[29] C. Zhao, X. Chen, C. Zhao, Y. Liu, Carbonation and hydration characteristics of dry potassium-based sorbents for CO2 capture, Energy Fuels 23 (3) (2009) 1766–1769, https://doi.org/10.1021/ef800889m.

[30] EU H2020 CREATE Project. EeB-06-2015, 2020. http://www.createproject.eu/.

[31] L. Sögütoglu, R. Bayer, J. Houben, H. Huinink, Composites Based on Potassium Carbonate for Thermochemical Energy Storage, 2020.

[32] R. Sander, Compilation of Henry's law constants (version 4.0) for water as solvent, Atmos. Chem. Phys. 15 (2015) 4399–4981, https://doi.org/10.5194/acp-15-4399-2015. www.atmos-chem-phys.net/15/4399/2015/.